

Structure of $\text{Ca}_{0.4}\text{K}_{0.6}(\text{NO}_3)_{1.4}$ from the glass to the liquid state

Charbel Tengroth,^{1,*} Jan Swenson,¹ Alessandro Isopo,² and Lars Börjesson¹

¹*Applied Physics, Chalmers University of Technology, S-41296 Göteborg, Sweden*

²*Dept. of Chemistry, INFN, University of Rome "La Sapienza," I-00185 Rome, Italy*

(Received 18 January 2001; published 21 November 2001)

We have investigated the structure of a model fragile glass former $\text{Ca}_{0.4}\text{K}_{0.6}(\text{NO}_3)_{1.4}$ (CKN) by using neutron and x-ray diffraction and reverse Monte Carlo modeling in a temperature range covering the glass transition. The results show that the structure of the glass phase contains, in addition to short-range charge ordering, intermediate-range ordering that is due to fluctuation of nitrate ion concentration in the range 3–15 Å. Furthermore, the nitrate ions are orientationally correlated and form chainlike substructures. Gradual changes of the structure factor were observed in the Q range 1–5 Å⁻¹ on passing through the glass transition temperature, which can partly be attributed to changes in density. However, the orientational correlation between the planar NO_3^- ions present in the glass phase is lost in the liquid phase.

DOI: 10.1103/PhysRevB.64.224207

PACS number(s): 61.43.Fs, 64.70.Pf, 87.64.Bx

INTRODUCTION

For glass forming liquids, below their melting points, the time scales of molecular motions and at which they respond to external perturbations increases dramatically with decreasing temperature. Eventually, the supercooled liquid will reach the glass transition temperature, which corresponds to the temperature at which the liquid appears “solid like”; i.e., the structural relaxation time is around 1000 s.

Extrapolations of experimentally determined structural relaxation times in the supercooled liquid suggest diverging time scales at a finite temperature below T_g . The way the motions slow down as the liquid freezes and forms a glass has been the subject of numerous investigations recently (see, for example Ref. 1), but remains an outstanding problem in condensed matter science. The slowing down of the dynamics in the supercooled range has been investigated by numerous dynamical techniques, e.g., neutron scattering, NMR, light scattering, dielectric spectroscopy, etc. (for a recent review, see, e.g., Ref. 2). In contrast, structural investigations are relatively scarce.³ This is probably due to that most investigations carried out on good glass forming liquids which show large dynamical effects close to T_g (i.e., fragile glass formers) are organic liquids, which are not ideally suited for x-ray or neutron diffraction since the hydrogen content complicates the analysis. Furthermore, diffraction data are to a large extent dominated by intramolecular or short-range correlations which normally do not exhibit any dramatic behavior on cooling a liquid through the supercooled regime.

However, most models and theories that have been put forward to explain the glass transition and dynamics of supercooled liquids make various assumptions about the behavior of the structure in the supercooled range or can be associated with various signatures. For example, there are a number of models that identify the slowing down of the dynamics with a growing length scale,^{4–6} a signature of critical phenomena. Support for a growing dynamical correlation length, or *cooperative rearranging region*, has been found in computer simulations of polymers and Lennard-Jones liquids⁷ and in studies of supercooled liquids confined to

nanopores or thin films.⁸ However, the experimental findings are not entirely conclusive since it is possible the confinement itself might induce changes in dynamics.

Other theories consider the glass transition to be kinetic in nature. One of the most interesting is the mode coupling theory (MCT), which gives detailed predictions on the dynamical behavior of the supercooled liquid around T_g . These predictions have been tested extensively by experiments in recent years.^{1,9} A common feature of kinetic models of the glass transition is that they assume that there is no thermodynamic transition associated with it and, consequently, that there are no sudden or large changes in the structure of the liquid as it solidifies into a glass. In most investigations aimed at testing MCT predictions, it has been assumed that no important structural changes occur in the supercooled range other than those given directly by the change of density.

Although there has been studies of glass structure, both by experiment, simulation, and computer modeling, there is little detailed work done on the structure of a liquid passing through the glass transition.^{3,10} We address this issue in the present study by investigating the structure of the archetypical “fragile” ionic glass former¹¹ $\text{Ca}_{0.4}\text{K}_{0.6}(\text{NO}_3)_{1.4}$ (CKN) at various temperatures around the glass transition ($T_g = 333$ K) using neutron diffraction and for $T = 300$ K also x-ray diffraction. The data have been used to model the atomic arrangements by means of the reverse Monte Carlo method.^{12,13}

CKN is a relatively simple ionic liquid whose structure and dynamics are governed by Coulomb interactions between the different constituents, with the added structural complexity of the triangular NO_3^- ion. The CKN glass former has previously been investigated with a multitude of dynamical probes in order to test the predictions of the much debated MCT. Former studies have concentrated on clarifying the dynamics around or below T_g and include inelastic neutron scattering experiments,^{14–16} neutron diffraction,¹⁷ Brillouin^{18,19} and Raman^{20,21} scattering, nuclear magnetic resonance,^{22,23} transient optical Kerr effect,²⁴ and molecular dynamics (MD) simulations.^{25,26} CKN shows extremely non-Arrhenius behavior, and the viscosity increases very rapidly

when approaching T_g from the high-temperature side. The aim of this study is to quantify to what extent changes in the structure can be related to the changes in density and if there are any other changes in the structure when the liquid freezes to a glass. To our knowledge the structure of neither the glass nor the liquid state of CKN has been investigated in any great detail by experiment before.

EXPERIMENT

Samples were prepared by using a standard melt quenching technique. Analytic grade KNO_3 and $\text{Ca}(\text{NO}_3)_2$ were heated slowly up to 573 K and kept at that temperature for several days in order to complete the removal of water. The sample was then quenched into a rod shape, 5 mm diameter and 50 mm long, and precautions were taken to avoid contact of the sample with air. The rod of $\text{Ca}_{0.4}\text{K}_{0.6}(\text{NO}_3)_{1.4}$ was placed in a thin-walled, cylindrical, vanadium can. The temperature-dependent neutron diffraction experiments were carried out at the SLAD (Studsvik Liquid and Amorphous Diffractometer) instrument at the Studsvik neutron research laboratory. Diffraction data were recorded in the range $0.3 < Q < 10.5 \text{ \AA}^{-1}$ at temperatures $T = 300, 333, 358,$ and 573 K. Another measurement was carried out at room temperature at the ISIS spallation source using the LAD instrument. The larger Q range available ($0.2\text{--}50 \text{ \AA}^{-1}$) was important for the determination of the NO_3^- molecular form factor. The data were corrected for background and container scattering, absorption, and inelastic and multiple scattering and normalized against the scattering of a vanadium rod.

Because of the relatively small contribution to the scattered intensity from the cations in CKN when using neutrons as an experimental probe, energy-dispersive x-ray diffraction (EDXD) measurements were carried out at room temperature. Contributions of the different pair correlations to the total structure factor in x-ray and neutron diffraction have been calculated and are presented below. For x-ray scattering (at $q=0$), the calculations give

$$S_x(Q) = 0.0204S_{\text{NN}}(Q) + 0.139S_{\text{NO}}(Q) + 0.047S_{\text{NK}}(Q) \\ + 0.033S_{\text{NCa}}(Q) + 0.240S_{\text{OO}}(Q) + 0.163S_{\text{OK}}(Q) \\ + 0.114S_{\text{OCa}}(Q) + 0.0276S_{\text{KK}}(Q) + 0.039S_{\text{KCa}}(Q) \\ + 0.136S_{\text{CaCa}}(Q)$$

and, for neutron scattering,

$$S_n(Q) = 0.09S_{\text{NN}}(Q) + 0.32S_{\text{NO}}(Q) + 0.031S_{\text{NK}}(Q) \\ + 0.028S_{\text{NCa}}(Q) + 0.32S_{\text{OO}}(Q) + 0.058S_{\text{OK}}(Q) \\ + 0.05S_{\text{OCa}}(Q) + 2.6 \times 10^{-3}S_{\text{KK}}(Q) + 4.5 \\ \times 10^{-3}S_{\text{KCa}}(Q) + 2.1 \times 10^{-3}S_{\text{CaCa}}(Q),$$

where the factors A_{ij} are given by the Faber-Ziman formalism²⁷

$$A_{ij} = \frac{c_i c_j \langle b_i \rangle \langle b_j \rangle}{\sum_i c_i \langle b_i \rangle^2}.$$

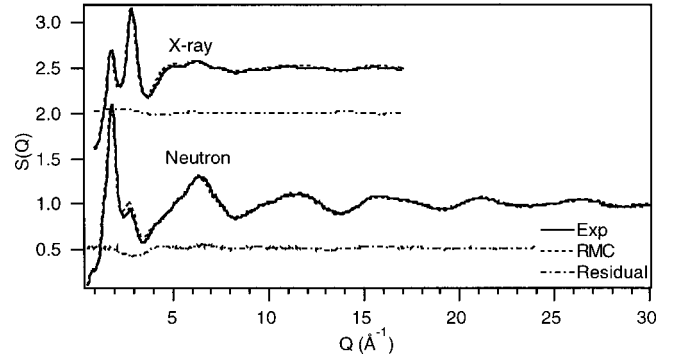


FIG. 1. Static structure factors $S(Q)$ obtained from x-ray (top) and neutron (LAD instrument) diffraction. The x-ray data have been shifted upward for clarity. Experimental data are shown as solid lines; dashed lines represent RMC fits to the data.

Here c_i is the concentration of atomic species i and b_i is the corresponding neutron scattering length or atomic form factor.

The method of EDXD consists of collecting the x-rays scattered from the sample at a fixed angle. The bremsstrahlung spectra produced by the collision of keV electrons on a tungsten anode is used as the polychromatic source of energy. The reciprocal space sampling is made electronically by each energy component of the primary beam. Applicability and advantages of the energy-dispersive method in the study of amorphous material has been widely described in the literature.^{28,29}

Measurements were carried out by employing a noncommercial x-ray scanning diffractometer in ϑ - ϑ symmetric configuration, constructed at the powder diffraction laboratory of the Chemistry Department of the University of Rome “La Sapienza.” The machine is composed of two rotating arms in the vertical plane, which can be moved independently in the range $5^\circ < 2\vartheta < 120^\circ$. The angular tolerance of the instrument is less than 0.005° . To reduce the angular divergence of both the incident and scattered x-ray beams, a set of four slits was suitably positioned along the arms. Each slit is made of a vertical and a horizontal pair of blades, adjustable in steps of $20 \mu\text{m}$. A more detailed description of the apparatus has been given in Ref. 30. Given the 13–39 keV energy range of the primary beam, the scattering intensity was obtained in the Q range $0.23\text{--}17.3 \text{ \AA}^{-1}$.

The sample in the form of a solid slab, 2 mm thick, was contained in a vacuum cell to prevent absorption of water. The cell was placed in the optical center of the diffractometer, which was defined through preliminary measurements. The measurements were carried out in transmission geometry in order to facilitate the sample absorption corrections.

EXPERIMENTAL RESULTS

Figure 1 shows the static structure factor at room temperature obtained from the LAD diffractometer and x-ray diffraction measurements. The oscillations of $S(Q)$ at $Q > 10 \text{ \AA}^{-1}$ are predominantly due to the intramolecular correlations of the NO_3^- ion, i.e., the N-O and O-O distances. We

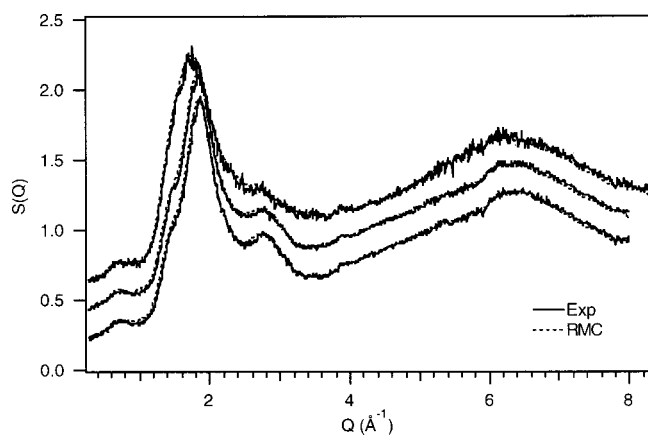


FIG. 2. Experimental static structure factor $S(Q)$ for temperatures $T=300, 358,$ and 573 K. Subsequent curves have been displaced vertically in steps of 0.2 for clarity. Thin lines represent RMC fits to the data.

observed no difference (within statistical accuracy) in the overlapping Q range when comparing data from the two neutron diffraction instruments at room temperature.

The static structure factors $S(Q)$ for $T=300, 358,$ and 573 K obtained from the experiments at SLAD are shown in Fig. 2. The $S(Q)$ obtained at 333 K was almost identical to that at 358 K, and this curve has therefore been omitted from the figure for clarity. As shown in Fig. 2, there are no dramatic changes of $S(Q)$ with temperature. However, the main peak at 1.9 \AA^{-1} and the smaller peak around 2.8 \AA^{-1} are significantly affected by the change in temperature. The main peak shifts to lower Q values and broadens, and the 2.8 \AA^{-1} peak loses intensity and moves to lower Q with increasing temperature. In contrast, the prepeak at 0.8 \AA^{-1} remains essentially unaffected. The remaining part of the structure factor is fairly constant throughout the temperature range, as has been observed in previous work: see Refs. 16 and 31. Thus the diffraction data of CKN display changes in the Q range where the interion correlation dominates on passing through the glass transition, whereas the intra- NO_3^- structure is largely temperature independent.

The NO_3^- intramolecular distances can be obtained directly from the neutron-weighted pair correlation function $G(r)$, the Fourier transform of the neutron $S(Q)$, shown in Fig. 3. The strong peak at 1.24 \AA is identified as corresponding to the N-O distance, while the second peak at 2.16 \AA comes from the nearest O-O distance in the nitrate ion. The distances confirm the planar triangular geometry of the ions with O-N-O angles of 120° . The main peak in $S(Q)$ at 1.8 \AA^{-1} (Fig. 1) appears to originate from an oscillation in $G(r)$ with a period of 3.5 \AA ($\approx 2\pi/1.8 \text{ \AA}$). The density fluctuations are clearly seen out to about 15 \AA (see inset in Fig. 3), suggesting a well-defined correlation between the nitrate ions: note the peaks at $r \approx 7.5, 11,$ and 14 \AA . The weak prepeak at 0.8 \AA^{-1} in $S(Q)$ should also contribute to the peak at about 7.5 \AA ($\approx 2\pi/0.8$) in $G(r)$ and to the oscillations further out in r (inset in Fig. 3).

REVERSE MONTE CARLO MODELING

For multicomponent glasses, it is normally difficult to extract quantitative structural information directly from the

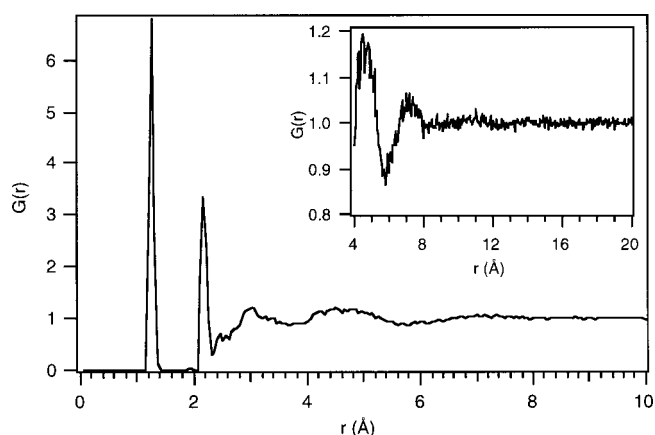


FIG. 3. Neutron-weighted pair correlation function $G(r)$ obtained from the Fourier transform of the experimental $S(Q)$ at $T=300$ K. The strong peak at 1.24 \AA denotes the N-O distance within the nitrate ion. The second peak at 2.16 \AA comes from the nearest O-O distance in the NO_3^- ion. The inset shows $G(r)$ at distances corresponding to the intermediate-range order. Note the different scale of the y axis.

static structure factor or radial distribution function, apart from the nearest-neighbor distances, due to strong overlap of peaks corresponding to different partial correlations. In order to better understand the structure of CKN, we have modeled the glass structure using the reverse Monte Carlo (RMC) method.^{12,13} The technique makes use of all the available structural data and does not require a model potential as for molecular dynamics and Monte Carlo simulations. The RMC simulation method has previously been used to successfully model the structure of network glasses, polymers, and other disordered systems.^{13,32-34} It uses the standard Metropolis algorithm, but instead of minimizing the energy, the difference between the experimental $S_e(Q)$ and calculated static structure factor $S_c(Q)$ is minimized. Any model configuration giving a diffraction pattern sufficiently close to the experimental $S(Q)$, i.e., within experimental errors, is a possible solution. In order to avoid unrealistic structures (e.g., atoms overlapping each other), we need to introduce constraints on the closest atom-atom approaches and coordination numbers of neighboring atoms. In CKN, the nitrate ion can be regarded as a basic structural unit: we therefore required every N atom to be surrounded by three oxygen atoms within the distance $1.2-1.3 \text{ \AA}$. The correct NO_3^- bond angles were obtained by constraining the O-O distance to $2.1-2.3 \text{ \AA}$ within the nitrate ions. The closest approach distances were based on ionic radii and structural information on the nitrate ion, obtained from Ref. 35 and the experimentally obtained $G(r)$ (see Fig. 3). The details are presented in Table I.

The simulated structure at room temperature was a cubic box, of 36.15 \AA side length, with 3300 atoms. Periodic boundary conditions were applied. The volume of the box was set to fulfill the experimental density of CKN at each temperature. The density values were taken from measurements by Dietzel and Poegel.³⁶ The nitrogen atoms were first introduced into the box, after which three oxygen atoms were added close to each nitrogen and subsequently moved out to ensure the correct distances and coordinations within

TABLE I. Nearest-neighbor distances applied in the RMC simulations. All distances are given in angstroms (Å).

Atomic species	N	O	K	Ca
N	3.0	1.2	2.4	2.4
O		2.1	2.2	2.2
K			3.6	3.6
Ca				3.6

the NO_3^- ions. Finally, the cations were randomly placed in the box, before the actual fitting to the experimental $S_n(Q)$ and $S_x(Q)$ at $T=300$ K was initiated. Two independent simulations were performed, one by fitting $S_c(Q)$ to room-temperature neutron and x-ray data simultaneously. The resulting structural model will then be relevant for both the NO_3^- , the cation, and the cross correlations. The other simulation was based only on the temperature-dependent neutron data. The configuration will therefore contain essential information on the temperature dependence of the nitrate ion structure, but will bear little information on the cation positions.

RMC RESULTS

The calculated $S_c(Q)$ is in near-perfect agreement with the experimental static structure factors, as can be seen in Figs. 1 and 2. Thus the configurations should contain essential information on the correlations giving rise to the various features in the $S_n(Q)$ and $S_x(Q)$, as well as the temperature-dependent features seen in Fig. 2. The structure factors from the RMC produced model structure at $T=300$ K and a random distribution model of the glass are shown in Fig. 4. The random distribution model deviates significantly from the RMC structure at Q values of the first and third peaks, while the location of the main (second) peak in the structure factor, related to the average nearest N-N distance (i.e., the density), is fairly well reproduced. This clearly shows that the structure of CKN is not particularly well described by the simple “dense random packing” (DRP) model,³⁷ which commonly

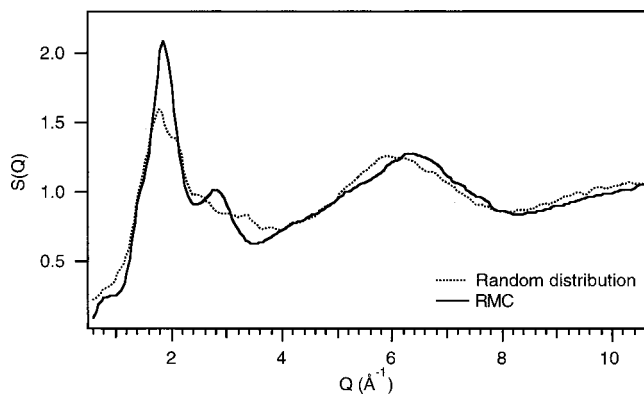


FIG. 4. Neutron-weighted static structure factors for the RMC-produced model based on neutron and x-ray data (solid line) and for the random distribution model (dashed line) we used as start configuration for the RMC model.

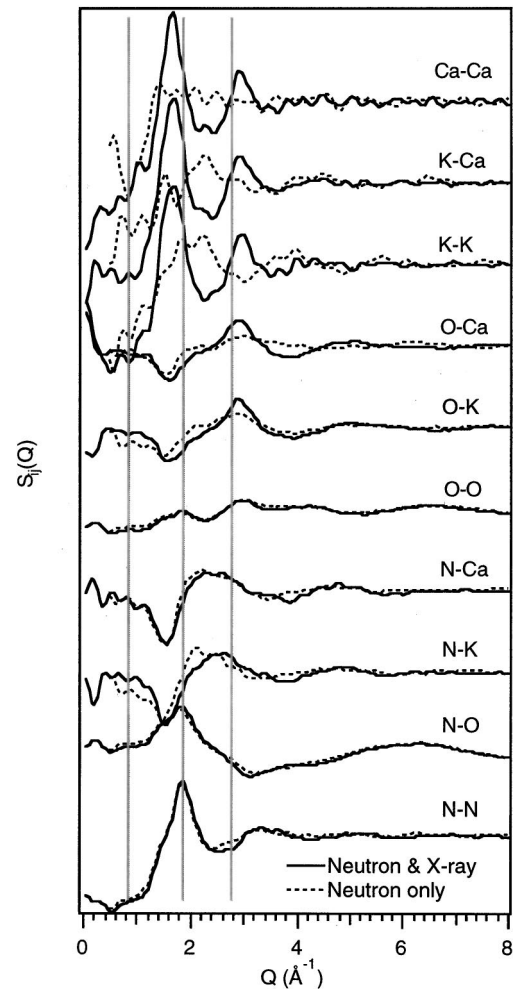


FIG. 5. Partial structure factors obtained from the RMC models at room temperature. The vertical lines show the positions of the diffraction peaks at 0.8, 1.85, and 2.8 \AA^{-1} . The solid lines correspond to the results from fitting to both neutron and x-ray diffraction data; dashed lines correspond to the RMC model based on neutron data only.

is believed to describe the structure of ionic solids and other amorphous materials with predominantly nondirectional interparticle forces.

The various atomic pair correlations can be obtained from the RMC result by calculating the partial structure factors and radial distribution functions. The partial static structure factors $S_{ij}(Q)$ are defined by the Faber-Ziman formalism through

$$S(Q) = \frac{\sum_{i,j} c_i c_j \langle b_i \rangle \langle b_j \rangle [S_{ij}(Q) - 1]}{\sum_i c_i \langle b_i \rangle^2} + 1,$$

where c_i is the concentration of atomic species i and b_i is the corresponding neutron scattering length or atomic form factor.

The $S_{ij}(Q)$ for the 300 K configuration obtained from $S_n(Q)$ and $S_x(Q)$ are presented in Fig. 5 (solid lines). The vertical lines show the locations in $S_n(Q)$ of the pre-peak, the first sharp diffraction peak (FSDP), and the second peak,

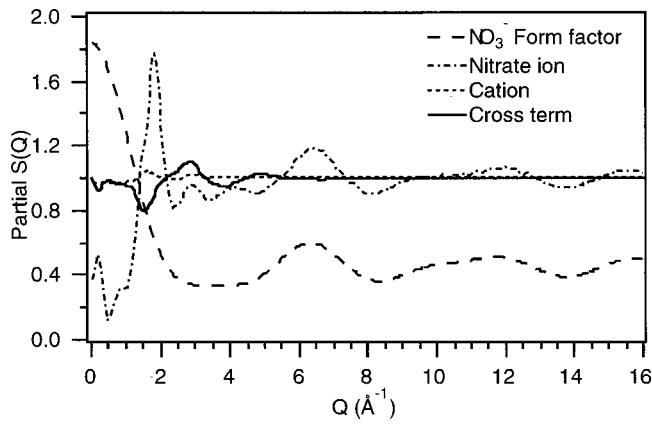


FIG. 6. Co-added neutron-weighted partial structure factors from the 300 K RMC simulation based on both neutron and x-ray diffraction data. The solid line contains the N-N, N-O, and O-O partial structure factors. The dash-dotted line contains the K-K, K-Ca, and Ca-Ca partial $S(Q)$'s. The dashed line is the sum of the N-K, N-Ca, O-K, and O-Ca partial $S(Q)$'s. Also shown is the calculated molecular form factor of the nitrate ion (displaced vertically). Note the agreement between the NO_3^- partial $S(Q)$ and the total $S(Q)$ from Fig. 1.

respectively, at 300 K. It is clear that the total neutron $S_n(Q)$ (Fig. 1) is similar to the N-N partial structure factor up to $Q = 2.2 \text{ \AA}^{-1}$, while the N-O partial $S(Q)$ dominates the experimental features at higher Q . Correlations involving the cations are clearly responsible for the strong peak at $\approx 2.8 \text{ \AA}^{-1}$ observed in the x-ray diffraction data (Fig. 2), especially the cation-cation and oxygen-cation correlations.

Figure 5 also displays a comparison between the configuration fitted to both neutron and x-ray diffraction data (solid lines) and the one obtained from fitting to neutron diffraction data only (dashed lines). Large differences are only evident in the $S_{ij}(Q)$ containing K^+ and Ca^{2+} correlations as expected from the lack of cation-specific information when no x-ray data are used. In the partial static structure factors containing nitrogen and oxygen correlations, no substantial differences are observed (see Fig. 5). Thus, in the investigation of the temperature dependence of the structure, only correlations involving the nitrate ion will be considered since we clearly lack detailed information about the cations at higher temperatures (neutron diffraction data only).

Let us first investigate the contributions of the partial structure factors to the main peaks in $S_n(Q)$. In order to focus on the main features and simplify our analysis, we group the ten $S_{ij}(Q)$ into three groups, weighting them according to their concentrations and neutron scattering lengths. The first grouped partial structure factor involves correlations within and between the NO_3^- ions (i.e., the N-N, N-O, and O-O correlations), the second grouped partial structure factor represents correlations between the cations (i.e., Ca-Ca, Ca-K, and K-K), and the third group partial structure factor contains the remaining cross correlations (i.e., N-Ca, N-K, O-Ca, and O-K). These grouped structure factors are shown in Fig. 6, together with the calculated atomic form factor of the nitrate ion. The nitrate ion form factor agrees well with the nitrate ion partial structure factor

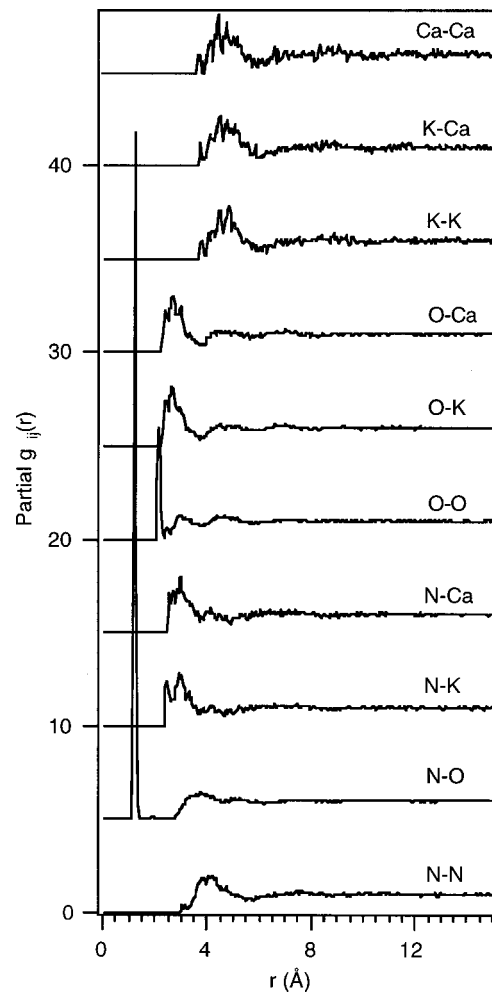


FIG. 7. Partial pair correlation functions obtained from the RMC-produced model structure based on neutron and x-ray diffraction data taken at $T = 300 \text{ K}$.

at wave vectors $> 3 \text{ \AA}^{-1}$, indicating that at smaller wave vectors the NO_3^- structure factor shows the interior correlations. The cation partial structure factor shows little contributions to the total $S_n(Q)$ at all Q , as expected from their low atomic concentrations. The peaks at 2.8 and 0.8 \AA^{-1} of the total structure factor both have contributions from the cross correlation, where we also see the charge ordering in the glass: the cross correlation has a maximum where the nitrate ion and intercation correlations have local minima and vice versa.

The partial pair correlation functions $g_{ij}(r)$ were also calculated from the RMC configurations. In Fig. 7 we show results from the configuration obtained from x-ray and neutron diffraction at 300 K. The N-N pair correlation function has a broad peak centered around 4.2 \AA : the width of the peak gives an idea of the distribution of nearest-neighbor NO_3^- distances. Due to the applied constraints of the well-defined intramolecular distances within the nitrate ion, the N-O and O-O pair correlation functions both have a sharp first peak. The second-nearest distance for the O-O pair correlation function shows an interesting “split-peak” behavior. This is an indication of an orientational correlation between

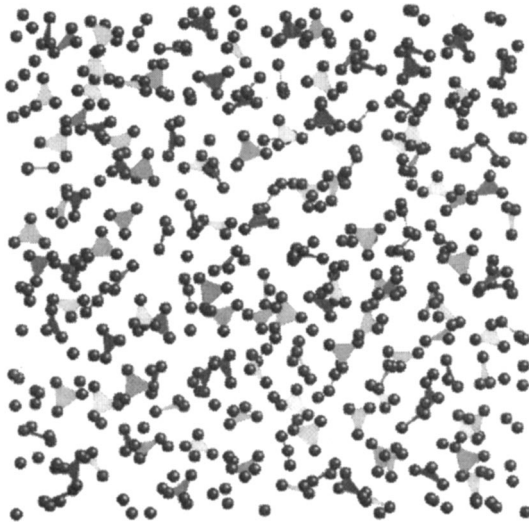


FIG. 8. RMC-produced structural model of CKN at room temperature. Presented is a slab with dimensions $37 \times 37 \times 10 \text{ \AA}^3$. The triangles represent NO_3^- ions with oxygen atoms as dark spheres. The potassium and calcium ions are not shown.

nitrate ions; consider two neighboring NO_3^- ions positioned so that two of the oxygen atoms in each molecule are facing each other (so that the third oxygen atom is at maximum distance from its counterpart). From Fig. 7 we obtain a distance of 3 \AA between the neighboring oxygen atoms (the position of the first hump in the split peak): the N-N distance is then $3 + 2 \times 1.24 \cos 60^\circ \approx 4.2 \text{ \AA}$, in perfect agreement with the position of the first peak in the N-N pair correlation function. The distance separating the two parts in the second peak of the O-O partial pair distribution function is 1.75 \AA , close to the calculated value for the separating distance of (approximately) $2.16 \cos 30^\circ \approx 1.9 \text{ \AA}$ between the two humps of the split peak. Had the oxygen atoms been oriented completely at random, one would have expected the second coordination shell to resemble the first peak of $g_{\text{NN}}(r)$, although broader. The interior distances obtained from the peaks in the $g_{ij}(r)$ presented in Fig. 7 are similar to those

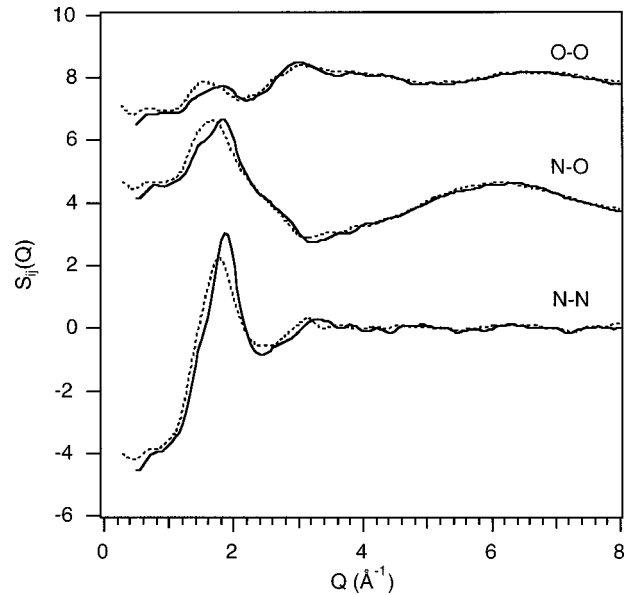


FIG. 9. Partial structure factors from $T=300 \text{ K}$ (solid line) and 573 K (dashed line).

reported in Ref. 26, although the shapes of the functions do not agree. Since the reported MD-calculated models do not show comparisons of the static structure factor with those obtained experimentally, it is difficult to assess the nature of this discrepancy.

A graphic representation of the calculated RMC model at room temperature is presented in Fig. 8. The K^+ and Ca^{2+} (not shown) take up space in between the aggregates of NO_3^- triangles. What is evident from this picture is the existence of structural heterogeneities in the material: i.e., there are variations in the local concentration of nitrate groups. We attribute this to the small peak in $S_n(Q)$ at 0.8 \AA^{-1} and the peak at 7.5 \AA in $G(r)$. Furthermore, the chainlike structures formed by neighboring nitrate ions are due to the orientational correlation observed as the split second peak in the O-O pair correlation function. Contrary to what has been suggested in earlier studies (see Ref. 26, and references

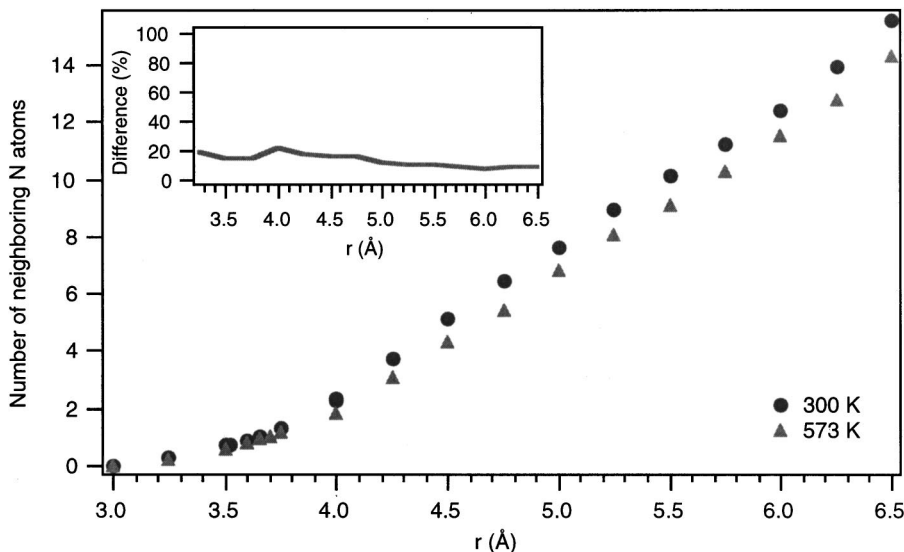


FIG. 10. The N-N coordination number as a function of r at $T=300$ and 573 K . The inset shows the relative differences between the two temperatures.

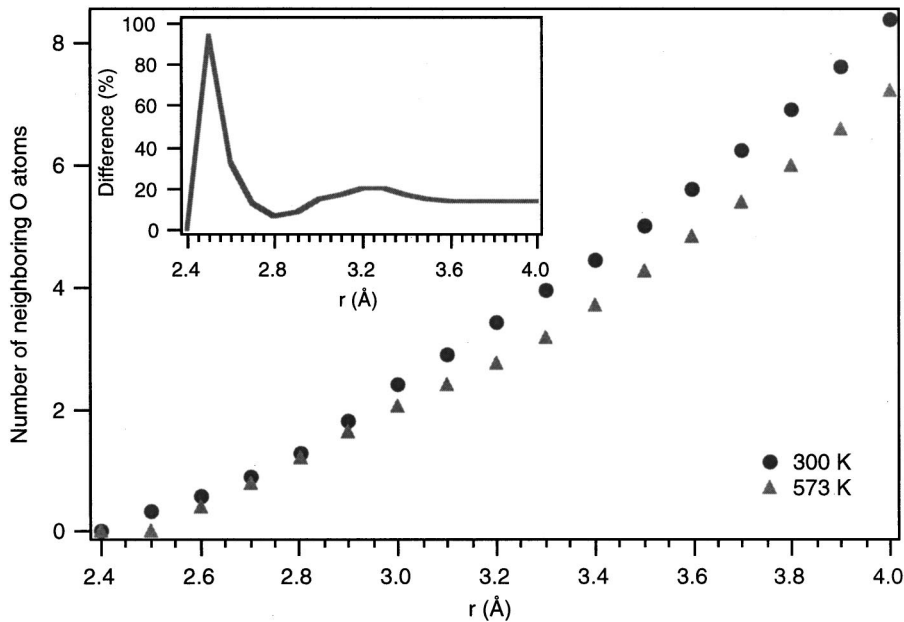


FIG. 11. The O-O coordination number as a function of r at $T=300$ and 573 K. The inset shows the relative difference between the two temperatures.

therein), there are no experimental indications of this prepeak being due to an intermediate range ordering of the cations; such an ordering would have been detected in the x-ray diffraction measurement because of its greater sensitivity to the cationic ordering. Experimentally, a small peak has indeed been observed at the expected value of momentum transfer,³⁸ but its small amplitude rules out the interpretation presented in Refs. 17, 25, and 26.

We now turn to the temperature dependence of the structure and consider first the contributions to the various peaks in $S_n(Q)$. Since only neutron scattering measurements were carried out at the higher temperatures, we do not have any significant information about the cations: hence, they are excluded from Fig. 9. The changes in the nitrate ion partial $S(Q)$'s (Fig. 9) with temperature were found to be gradual throughout the whole temperature range: only the partials obtained for the highest and lowest temperatures are shown. From the figure it is clear that all the partial structure factors of the NO_3^- ion (N-N, N-O, and O-O) have a peak around 1.8 \AA^{-1} that is shifted to lower Q values upon raising the temperature. Thus the shift of the main peak in the total $S_n(Q)$ comes from an increased internitrate ion distance. The origin of the vanishing peak at 2.8 \AA^{-1} can also be deduced from Fig. 9; the second peak in the O-O partial $S(Q)$ displays a loss of intensity in that Q region. There might also be a loss of oxygen-cation correlation in this region of Q as well.

From the RMC structures, coordination numbers of the different partial correlations have been calculated. Results for the N-N and O-O coordination numbers as a function of radius r are presented in Figs. 10 and 11. The inset shows the ratio between the coordination numbers obtained from the room-temperature data and 573 K configurations. The N-N coordination number, $n_{\text{N-N}}(r)$, is steadily increasing for increasing r and with an almost constant relative difference between the two temperatures. However, it should be noted that the relative difference is about 20% (i.e., twice as much as the average density difference) for r up to about 4.5 \AA and the average density difference is not reached until $r \approx 6 \text{ \AA}$

(see inset of Fig. 10). In the case of $n_{\text{O-O}}(r)$ (Fig. 11), the difference for different temperatures is substantial in the immediate vicinity of the nearest oxygen atom distance ($r \approx 2.5 \text{ \AA}$) and, also, for slightly longer distances (the inset at $r \approx 3.2 \text{ \AA}$). Beyond that, the relative difference between the two curves stabilizes and follows a behavior close to that of $n_{\text{N-N}}(r)$ in Fig. 10. The two neighboring oxygens from the same nitrate ion have been subtracted from the results presented in Fig. 11 and do not contribute to this graph.

DISCUSSION

As shown in Fig. 6, the structure factor of CKN as observed by neutron scattering is to a large extent the structure of the nitrate ions. In order to understand the changes of the structure with temperature, it is of interest to elucidate the origins of the main features of the structure factor, in particular the three first peaks which to a significant extent should be due to internitrate ion correlations. It is clear that the N-N partial $S(Q)$ dominates the shape of the total $S(Q)$ up to $Q = 2 \text{ \AA}^{-1}$, although the FSDP at 1.8 \AA^{-1} has contributions from the N-O and O-O partial structure factors as well. There is also evidence of intermediate-range order. This is manifested by the small peak at 0.8 \AA^{-1} , seen in the N-N partial $S(Q)$.

The change in density when going from room temperature to 573 K is about 10%.³⁶ We therefore expect the N-N coordination number to differ about 10% between the 300 and 573 K curves. From the inset of Fig. 10, we see that this is indeed true for $r > 6.0 \text{ \AA}$. At closer distance, the difference is larger: up to 20%. We attribute this to an inhomogeneous thermal expansion in the material; the nitrate-cation distances are stabilized by the Coulomb interactions and will not increase as much as nitrate-nitrate ion distances upon heating. This difference is local (it extends not far beyond the nearest nitrate-nitrate ion distance) and is averaged out at larger distances, as expected. The inset in Fig. 11 reveals relatively large changes in the local environment of oxygen

between the glass and liquid. Since there is no evidence of such rearrangements between nitrogen atoms (the inset of Fig. 10 is rather flat), the changes must be due to in-plane rotation of the triangular nitrate ions. In the glass the oxygen atoms, sitting on the corners of the nitrate ion triangles, are to a certain extent orientationally correlated with each other. This orientational correlation is also seen as a double peak in the second coordination shell of the O-O pair correlation function (Fig. 7). The smearing out of this feature at higher temperatures shows that the orientational correlation is at least partly lost in the liquid phase. Although the effect is small, it must be stressed that the difference with temperature in the O-O pair correlation seen in Fig. 9 is most likely an underestimate of the real difference, since the RMC method tends to produce the most disordered structure that is in agreement with the experimental data.

The scenario of the structural rearrangements connected to the liquid-glass transition in CKN can thus be described as follows. In the high-temperature regime, the nitrate ions rotate quite freely, as has been seen in Raman, NMR, and transient optical Kerr effect (OKE) measurements.^{20,22–24} As the temperature approaches T_g , the density increases and this motion becomes hindered, resulting in nitrate ions with their relative orientations distributed in a nonrandom fashion, such that the oxygen atoms of neighboring nitrate ions are facing each other, resulting in a networklike structure of nitrate ions.

CONCLUSIONS

We have carried out diffraction experiments on the archetypical “fragile” ionic glass $\text{Ca}_{0.4}\text{K}_{0.6}(\text{NO}_3)_{1.4}$ at tempera-

tures ranging from 300 to 573 K. The aim was to investigate the possibility of structural changes when going from a glass to a liquid, other than those directly related to the thermal expansion and change in density. From the RMC-produced model configurations, we were able to study the local environment around the nitrate ions in CKN. This revealed the existence of an orientational correlation of the planar nitrate ion in the glass, with pairs of oxygens belonging to neighboring nitrate ions showing a preference of facing each other in the glassy state. At 573 K we were not able to observe any such orientational order. Furthermore, the diffraction data show the presence of intermediate-range order in the glass as well as in the liquid. This is unexpected considering that CKN is an ionic liquid, and no intrinsic directional bonds between positive and negative ions are expected. We find no support for the suggestion that the intermediate-range order should arise from cation correlations. Based on the RMC-produced model structures, the nitrate ions are inhomogeneously distributed and seem to cluster in chainlike aggregates.

ACKNOWLEDGMENTS

The authors wish to acknowledge fruitful discussions with Robert McGreevy on the RMC results. The neutron diffraction experiments were carried out with the help of Spencer Howells (ISIS) and Anders Wannberg (Studsvik). This work has been supported by the Swedish Natural Science Research Council (NFR).

*Present address: Dept. of Chemistry, Princeton University, Princeton, New Jersey 08544.

¹*Proceedings of the 3rd International Discussion Meeting on Relaxations in Complex Systems* [J. Non-Cryst. Solids, **235–237** (1997)].

²M. D. Ediger, C. A. Angell, and S. R. Nagel, J. Phys. Chem. **100**, 13200 (1996).

³R. L. Leheny, N. Menon, S. R. Nagel, D. L. Price, K. Suzuya, and P. Thiyagarajan, J. Chem. Phys. **105**, 7783 (1996).

⁴E. Donth, Acta Polym. **50**, 240 (1999).

⁵M. H. Cohen and D. Turnbull, J. Chem. Phys. **31**, 1164 (1959).

⁶G. Adam and J. H. Gibbs, J. Chem. Phys. **43**, 139 (1965).

⁷C. Bennemann, C. Donati, J. Baschnagel, and S. C. Glotzer, Nature (London) **399**, 246 (1999).

⁸H. Sillescu, J. Non-Cryst. Solids **243**, 81 (1999).

⁹A. P. Sokolov, Science **273**, 1675 (1996).

¹⁰R. Fayos, F. J. Bermejo, J. Dawidowski, H. E. Fischer, and M. A. González, Phys. Rev. Lett. **77**, 3823 (1996).

¹¹C. A. Angell, J. Non-Cryst. Solids **131–133**, 13 (1991).

¹²R. L. McGreevy and L. Puztai, Mol. Simul. **1**, 359 (1988).

¹³D. A. Keen and R. L. McGreevy, Nature (London) **344**, 423 (1990).

¹⁴F. Mezei, J. Non-Cryst. Solids **131–133**, 317 (1991).

¹⁵F. Mezei and M. Russina, J. Phys.: Condens. Matter **11**, A341 (1999).

¹⁶E. Kartini, M. F. Collins, B. Collier, F. Mezei, and E. C. Svensson, Phys. Rev. B **54**, 6292 (1996).

¹⁷E. Kartini, M. F. Collins, B. Collier, F. Mezei, and E. C. Svensson, Can. J. Phys. **73**, 748 (1995).

¹⁸G. Li, W. M. Du, X. K. Chen, H. Z. Cummins, and N. J. Tao, Phys. Rev. A **45**, 3867 (1992).

¹⁹L. M. Torell and R. Aronsson, J. Chem. Phys. **78**, 1121 (1983).

²⁰P. Jacobsson, L. Börjesson, A. K. Hassan, and L. M. Torell, J. Non-Cryst. Solids **172–174**, 161 (1994).

²¹E. Rössler, A. P. Sokolov, A. Kisliuk, and D. Quitmann, Phys. Rev. B **49**, 14 967 (1994).

²²S. Sen and J. F. Stebbins, Phys. Rev. Lett. **78**, 3495 (1997).

²³S. Sen and J. F. Stebbins, Phys. Rev. B **58**, 8379 (1998).

²⁴M. Ricci, P. Foggi, and R. Righini, J. Chem. Phys. **98**, 4892 (1993).

²⁵G. F. Signorini, J.-L. Barrat, and M. L. Klein, J. Chem. Phys. **92**, 1294 (1990).

²⁶M. C. Ribeiro, Phys. Rev. B **61**, 3297 (2000).

²⁷T. E. Faber and J. M. Ziman, Philos. Mag. **11**, 153 (1965).

²⁸R. Caminiti, M. Carbone, G. Mancini, and C. Sadun, J. Mater. Chem. **8**, 1331 (1997).

²⁹J. M. Prober and J. M. Schultz, J. Appl. Crystallogr. **8**, 405 (1975).

³⁰R. Caminiti, C. Sadun, V. Rossi, F. Cilloco, and R. Felici, XXV National Congress of Chemical Physics (Cagliari, 1991).

- ³¹C. Tengroth, J. Swenson, and L. Börjesson, *Physica B* **234–236**, 414 (1997).
- ³²J. Swenson and L. Börjesson, *J. Non-Cryst. Solids* **232–234**, 658 (1998).
- ³³J. Swenson, R. L. McGreevy, L. Börjesson, and J. D. Wicks, *Solid State Ionics* **105**, 55 (1998).
- ³⁴P. Carlsson, J. Swenson, L. Börjesson, L. M. Torell, R. L. McGreevy, and W. S. Howells, *J. Chem. Phys.* **109**, 8719 (1998).
- ³⁵R. D. Shannon, *Acta Crystallogr., Sect. A: Cryst. Phys., Diffr., Theor. Gen. Crystallogr.* **32**, 751 (1976).
- ³⁶A. Dietzel and H. P. Poegel, 3rd International Glass Congress (Venice, 1953).
- ³⁷J. D. Bernal, *Nature (London)* **183**, 141 (1959).
- ³⁸A. Matic, D. Engberg, C. Maciovecchio, G. Monaco, and L. Börjesson (unpublished).